

ENPH 454 Advanced Engineering Design Project

The Use of Eddy Current Testing for Defect Detection in Additive Manufactured Metals

Fei Han, Steven Hill, Ronald Rout, Daniel Tettmann, Matthew Tidman

December 5th 2021

Instructor: Robert Knobel

Instructor: James Stotz

Teaching Assistant: Colin Moore

Abstract

The non-destructive method of electromagnetic eddy current testing is investigated using mirrored D-shaped coils and a giant magneto resistor sensor. An AC current between 1 – 5 kHz was sent through the coil wires generating a magnetic field oriented as if it were a single solenoid. Various samples were measured consisting of aluminum, copper, and brass, each type of metal had a sample with a $5/32^{\text{th}}$ diameter hole, a $5/16^{\text{th}}$ diameter hole, and a thin 0.18 mm depth surface crack. The sample defects under examination were used to mimic defects that would be present in the metal additive manufacturing process, specifically laser powder bed fusion methods. Although the defects under consideration are considerably larger than those encountered in the additive manufacturing process, the following research serves as a proof of concept that higher sensitivity sensors could be achieved. A linear actuator was used to create 1D scans of the surfaces of the metals, to detect the various defects. Tests were conducted for each defect type, along with detecting the large and small holes beneath another 'defect-free' sample to mimic the subsurface flaws.

Table of Contents

Abstract	<i>i</i>
1.0 Introduction and Background	1
2.0 Design Decisions	3
2.1 Coil and Detector Design.....	3
3.0 Safety, Environmental Concerns, Ethical Concerns, Equity	5
3.1 Construction assembly	5
3.2 Hazards During Testing and Operation	6
3.3 Environmental Considerations	6
3.4 Ethical Considerations	6
4.0 Methodology	7
4.1 Test Stand Design	8
4.2 Final Setup	11
5.0 Results	12
6.0 Discussion	17
8.0 Economic Analysis	19
8.1 Sensor Materials	19
8.2 Testing Materials	19
9.0 Conclusion	20
References	21
Appendices	1
Appendix A: Models	1
Appendix B: Printer Settings and Materials Cost.....	3
Appendix C: Data Acquisition Code:	5

1.0 Introduction and Background

There exists a need in research and manufacturing applications for methods that inspect material geometries. Numerous such methods exist, each possessing its own strengths and weaknesses. One class of inspection techniques, non-destructive testing (NDT) techniques, are particularly valuable given their ability to inspect objects themselves as opposed to similar models. This is important in applications where minuscule differences between similar models will appreciably affect their viability. It also eliminates the costs associated with partially or completely destroying a material during an inspection.

Within the area of NDT, commonly used methods include electron microscopy, x-ray techniques and eddy current testing (ECT). Electron microscopy, while providing reliable results, is conducted with a large apparatus and needs to be performed in a vacuum. This complicates its uses in research and makes it either difficult to use, or unfeasible, in manufacturing applications. X-ray techniques also require large apparatuses to operate, making them impractical for many applications. ECT conversely, does not need a large apparatus to operate, nor does it need to operate in a vacuum.

For this project, the team sought to inspect, non-destructively, the material geometries of thin sheets of metal. The motivation behind this project was to design an apparatus capable of detecting defects in layers of metal typically seen throughout the process of 3D printing metal parts. Typical defect sizes in additive manufactured metals: 50 micron gas pores, & fatigue cracks caused by such pores up to several microns in thickness [1]. Attaching our apparatus to a 3D printer to conduct scanning after each layer of metal is deposited is beyond the scope of the term-long project. Nevertheless, it was the team's aspiration that the design implemented would serve as the starting point for the development and implementation of such a device.

For the reasons listed above, the best method for achieving this aim was ECT. To conduct ECT, an alternating current is run through a solenoid that is placed near the test sample. The current moving through the solenoid induces a magnetic field, which in turn induces currents in the test sample. These currents are called eddy currents. They vary according to the material geometry of the test sample. The eddy currents in the test sample will induce a second magnetic field, which will also vary according to the sample's material geometry. This means that any

cracks, pores or holes should cause the magnetic induced to deviate from that which would be induced by a flawless sample.

The ability of ECT to successfully inspect a sample depends on several factors. To fully inspect a sample, the penetration depth of the sample must be equal to or greater than the thickness of the sample. The penetration depth is inversely proportional to the roots of the conductivity and magnetic permeability of the sample, and to the root of the frequency of the eddy currents[2]. This is shown in the equations below:

$$d = \frac{1}{\sqrt{f\pi\sigma\mu}} \quad (1)$$

Where d is the depth, f is the frequency of the current, σ is the conductivity of the test sample and μ is the magnetic permeability of the test sample.

The magnetic field induced by a solenoid is influenced by the latter's radius, length, number of turns, and orientation. For a single-coil solenoid with its central axis being the x-axis as shown in Figure 1, equations (2) and (3) show the magnetic field.

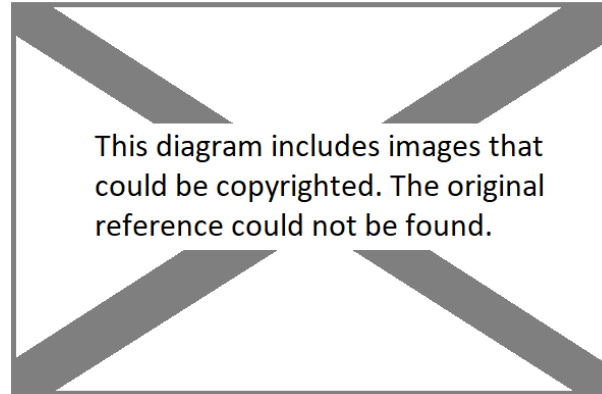


Figure 1: On left, a solenoid with its central axis located on the x-axis and ends at x_1 and x_2 . This solenoid corresponds to the solenoid whose magnetic field is shown in equation (2) and (3). On the right, the magnetic field strength in the x-direction is shown as a function of x-position.

$$B_x = \frac{\mu_0 n I}{2} R^2 \int_{x_1}^{x_2} \frac{dx'}{[(x - x')^2 + R^2]^{1.5}} \quad (2)$$

$$B_x = \frac{\mu_0 n I}{2} \left(\frac{x - x_1}{((x - x_1)^2 + R^2)^{0.5}} - \frac{x - x_2}{((x - x_2)^2 + R^2)^{0.5}} \right) \quad (3)$$

It must also be noted that two D-shaped coils oriented as shown in Figure 2, with a single current between the two, acts as a single solenoid [3]. Further, this configuration has experimental advantages that will be summarized below in *Design Decisions*.

Once eddy currents have induced a magnetic field, the next step in the ECT process is the measurement of these fields. This is accomplished by a magnetometer, usually either a giant magneto-resistor (GMR) sensor or a tunnel magneto-resistor (TMR) sensor. A GMR sensor is composed of a thin layer of a non-magnetic conductor, typically copper, sandwiched in between two layers of a ferromagnetic material. The resistance in the small conductive layer will decrease significantly as electron scattering occurs. This happens when the relative electron spin orientations surrounding the conducting layer (in the ferromagnetic layer) are subject to a magnetic field. The magnitude of the resistance change allows the magnitude of the magnetic field produced by the eddy currents to be deduced [4].

TMR sensors similarly possess two ferromagnetic layers. However, where a GMR sensor possesses a non-magnetic conductor, TMR sensors possess an insulator. The insulator sandwiched between the ferromagnet is called a *magnetic tunnel junction*. When a magnetic field is applied such that the direction of magnetizations of the ferromagnets is aligned in a parallel fashion, there is a small current that flows through the tunnel. This current increases with increasing magnetic field strength. Conversely, when the magnetizations are aligned in an anti-parallel manner, the electric current decreases as the resistance across the tunnel increases. This increase in resistance is proportional to the magnetic field strength [5].

The team ultimately chose to conduct the measurements with a GMR given advantages detailed in the *Design Decisions* below.

2.0 Design Decisions

Several major design considerations were taken to validate the design and construct a rigorous testing apparatus.

2.1 Coil and Detector Design

The sensor design consisted of two mirrored D-shaped copper coils, along with a GMR sensor placed at the center of the two coils, seen in Figure 2. Variation of the current flow direction between the two coils allows for two modes of operation. The currents flowing in phase

correspond to a magnetic field generated from the center of one coil through the other or emerging from the top of both, to wrap around the lengths and return to the bottom. The latter option was chosen, where the current ran in counterclockwise loops through each of the coils, because it was found to have better defect detection in the test samples. The inspiration for this design was found in the literature [3], as it has been experimentally proven to demonstrate good localization and defect detection in metallic samples [6]. Following from Section 1.0, the strength of the magnetic field is inversely proportional to the radius of the coil. Under the approximation that the two coils with current flowing in phase generate a similar magnetic field as if it were a single coil, the distance between the coils needed to be minimized.

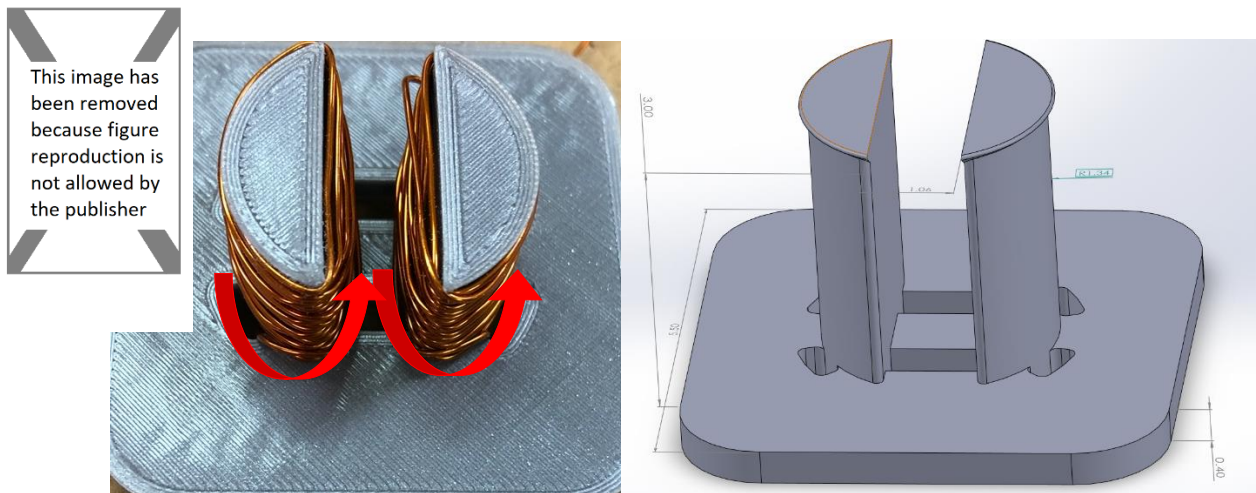


Figure 2: Left: Coil design used to generate eddy currents in the test probe, and sketch of the two different operation modes [6]. The top image shows the coils operating in phase, where the bottom shows the out of phase mode. The red arrows indicate the direction of current flow. Right: The CAD model used for 3d printing is in the image on the right. At the top there's a small extension at the top to hold the coils. And the holes made at the bottom plate is for a stronger printed part.

The GMR (AAL002-02E from NVE) detector was placed at the center of the two coils, where the relative strength of the magnetic field would be at its strongest. GMRs were chosen over TMRs as they have a higher maximum frequency which allowed for better testing of thinner metals, since the skin depth is inversely proportional to the square root of the frequency as shown in equation 1. TMRs had a maximum frequency of 50 – 1000 Hz, this was too low as it would give a much higher sink depth penetration than what we were planning to use, GMRs had a maximum frequency of 50 kHz – 5 MHz which allows us to work in the planned frequencies [7], [8]. For testing the 1.00-1.30 mm sheets this was in the range of 1-5 kHz however for real metal deposition the layers are much smaller, the GMR we used could have a skin depth as low

as 0.04 mm in aluminum. This is within the 0.03-0.1mm range of thickness in which aluminum is generally printed [9].

A lock-in amplifier (SR810 from Stanford research systems) was used to read the signal from the GMR. It was chosen because it can read signals on the order of a few nanovolts which allows for the detection of very small changes in the magnetic field. The lock-in amplifier also will only read the signals at the same frequency as those generated by the coil which removes much of the noise that would be present. In practice, the reading that was measured were in the microvolt range. The lock-in amplifier also generated the signal to the coils, it allowed for simple changing of the frequency and amplitude of the signal while also operating in the desired ranges. The lock-in amplifier had a maximum frequency of 10 kHz which is sufficient for the thickness of the test samples used.

The team choose to use fused deposition modelling (FDM) technology for 3D printing as a fast-prototyping method for producing the structure that holds the sensor at a precise location with a wide range of freedom. The design of the structure needs to allow the sensor to adjust its XYZ positions for consistent readings from the eddy currents generated.

3.0 Safety, Environmental Concerns, Ethical Concerns, Equity

The following supplementary concerns are discussed below. While some concerns such as safety changed design decisions and procedures, others serve as motivation for the testing.

3.1 Construction assembly

There was not any significant risk when constructing the structure for the testing. The biggest risk that occurred during the construction of the sensor was the soldering of wires and chips, as a team member could have gotten burned when interacting with a soldering iron. To protect team members during soldering, the team members wore goggles and gloves to protect their eyes and hands from being burnt.

The largest risk associated with the project involved manufacturing the test samples which were done in the machine shop. Band saws and drill presses were used which can both pose serious harm to the user if used incorrectly. To avoid casualties, the safety guidelines and rules during the safety training were followed, and the machinists were often consulted to oversee, or

advise during the use of the band saw specifically, which was used to make the cracks in the various samples.

There was no significant risk with the voltage (12.0 V) to be used for the magnetic coils.

3.2 Hazards During Testing and Operation

During the testing and operation of our apparatus, risks will emerge from the presence of electricity and magnetic fields. These risks are all preventable by adhering to basic safety protocols as outlined below.

From electricity, there are the hazards of electrical shock and/or burns. As is demanded by the Stirling laboratory rules, the team strictly abided by ensuring no water or similar fluids be near the apparatus. Team members also avoid touching the apparatus when it is live. Additionally, the team ensured that the signal generator was operated with grounded power cords. This was to prevent the potential for dangerous charge build-ups or ground-fault currents.

As for the magnetic fields, the team had ensured that objects subject to being significantly disturbed by the fields were kept away from the apparatus to avoid creating projectiles. It should be noted that this is unlikely to happen given the strength of the intended magnetic fields. The precaution was taken nonetheless, in case an error is made that results in a larger than expected field. This consideration had a larger effect on skewing the data than a serious safety concern.

3.3 Environmental Considerations

A large part of the motivation for this study was to be able to monitor the progress of additive manufactured parts for defects while the manufacturing process occurred layer by layer. The purpose of such testing is to avoid completing printed parts that have a defect density that affects the structural properties of the part. By allowing for real time monitoring, less wasted material would be produced for poorly manufactured parts by realizing any major defects that could occur along the process.

3.4 Ethical Considerations

A major part of engineering is upholding the code of ethics in the professional engineer's act, which ensures the safety and reliability of products for the general public. By allowing for cost-

efficient, real-time testing, the structural integrity of each product can be assessed at the time of manufacturing. This saves a great deal of resources required to test products either in a lab or using expensive X-ray equipment for reliability. With real time monitoring, the manufacturers will be more confident in each part, with better assurances in the reliability of their products.

4.0 Methodology

To validate the design of the sensor, test samples were made to mimic defects in additive deposition manufactured metals, namely subsurface pores, and cracks. The test samples were made from aluminum, copper, and brass, each with a large, 5/16th diameter hole, a small 5/32th diameter hole, and a 0.18 mm deep by 1.63 mm wide crack. Due to errors in manufacturing, the brass plate specifically had two cracks beside each other. This was not later corrected because a brass sheet was ordered specifically for testing purposes. The correction would involve either ordering more of the brass sheet, which time nor budget constraints allowed for, or the alternative, remaking the sample using spare brass found in the machine shop. However, no simple method was available to determine the grade of the brass, which may not have been comparable to the other samples. The samples were measured and compared to a defect free surface as a threshold to determine the driving frequency of the coils.

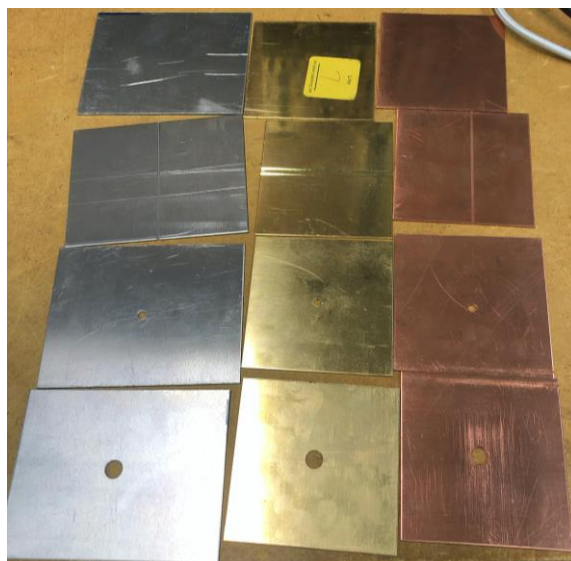


Figure 3: Left to right: aluminum, brass, and copper samples, with imposed defects.

During the testing stage, the team sought to obtain data reflective of the material geometries being tested (holes, cracks, etc.). The team also aimed to verify that the measurements had reproducibility, that is one sample would produce the same data each time it was tested. The results showed clear indications of the material geometries, with the output signal decreasing as holes and cracks were brought underneath the sample. However, the team realized that our detector had fluctuations even when no samples were being tested. This was seen as a clear impediment to obtaining reproducible results. After some consideration, it was thought that the presence of people moving near the sensor was affecting the readings. This was thought to be due to capacitive effects. To resolve this issue the addition of a faraday cage enclosing the test apparatus was used. Once the apparatus was covered with the faraday cage, the fluctuations that had previously been observed no longer appeared.

When testing, it was also found that a large amount of noise was present when the samples were on the stand but not when they were being held. It was determined that was due to the capacitance of the plates. To fix this the plates were placed on a grounded piece of copper tape, this removed the significant noise from the data.

The frequencies of the coil were changed depending on the material that was being tested. As different materials had different conductivities unique frequencies were need so that the depth penetration of the magnetic field was equal to the thickness of the sample, allowing the sensor to scan the whole sample and minimized reading cause by materials under the sample. These frequencies were found using Equation (1). These frequencies both dictated the signal going to the coil and the frequency that the lock-in amplifier read from the GMR. The voltage to the coil and to the GMR sensor were both set to their maximum, 5 V and 12 V respectively, to maximize the produced signal. This is because there was a constant noise when reading lower voltages so increasing the magnitude of the signal gave cleaner results. In order for the GMR to receive the 12 V supply, an independent regulated DC power supply was used.

4.1 Test Stand Design

To set up the structures for the experiment, the first parameter to be considered is the height. The sensor and the samples need to be raised up from the stepper motor to be affected less by the

magnetic field produced by it. The two pillars will sit flush with the rail of the linear actuator – used to move the samples against the detector probe during testing, for a stable setup. The beam is designed to be arched over the rail and to raise the sensor even more. The cut off in the middle allows the sensor to adjust the y-axis position with 10 cm of range. And the part that fixes the sensor structure also has 2.5 cm of vertical range. The sensor support assembly was made in as shown in Figure 4.

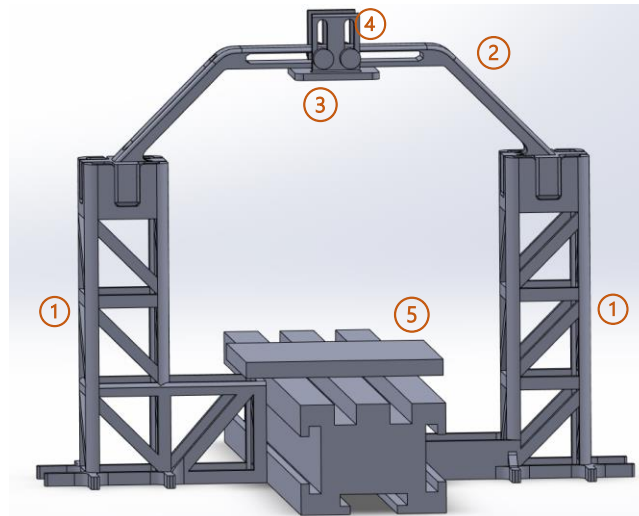


Figure 4: The structure section for sensor positioning. 1: Truss framed pillar. The one on the right has lowered contact height is to avoid the side that has a wire running along the rail. 2: Supporting beam. 3: Sensor positioning plate. 4: Nut and screws that holds the sensor positioning plate. Replaced with Lego pieces in the actual experiment. 5: linear actuator with the Sample pedestal.

The samples will be raised up with three components. The first one is the support plate being fixed on the moving platform with threads. The second component is a thread that will rotate on the male thread to adjust height. The third component will be the plate holding the samples and its height will be adjusted with the moving thread.

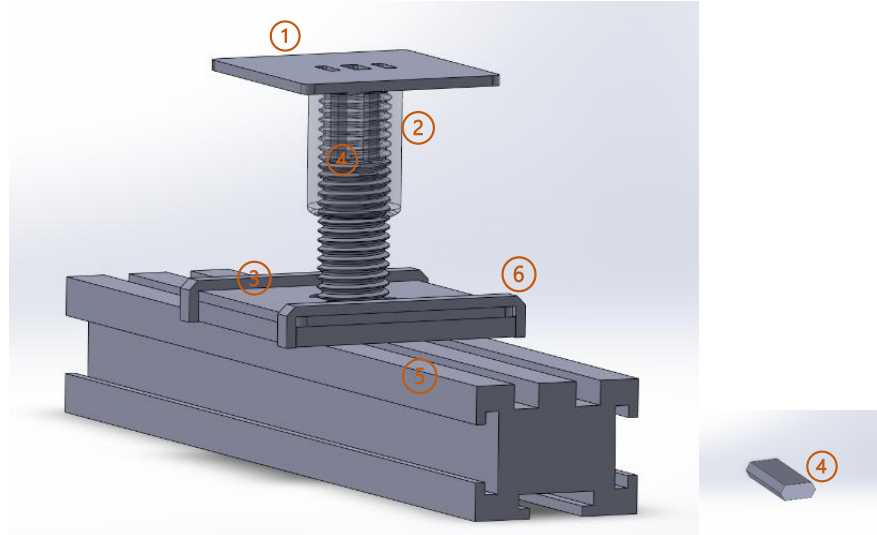


Figure 5: 1: The sample plate. 2: Height adjustment thread, shown transparent in figure. 3: Sample support structure. 4: Stopper that prevents the sample plate from sliding out after reaching maximum height. The CAD model is showing on the right and was never used because the maximum height was never reached. 5: linear actuator with the Sample pedestal. 6: The structure that holds down the sample support structure. In the experiment, they were replaced by plastic clamps.

When the sensor support structure was assembled with the sample support structure on the linear actuator, the testing environment was mostly complete. The final design was optimized for testing rather than production.

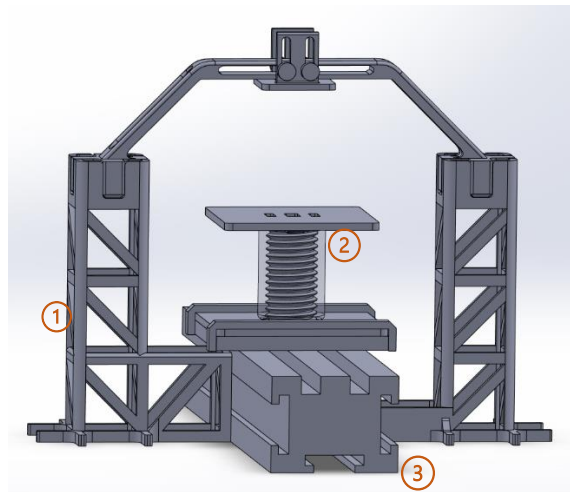


Figure 6: Cad design of test frame with outline of linear actuator. 1: Sensor support frame. 2: Sample support structure. 3: Sample pedestal

To hold the sensor and coils, the coil support structure was designed for wrapping the coil and fix it in place. A sensor bracket was made to fix the sensor in place.

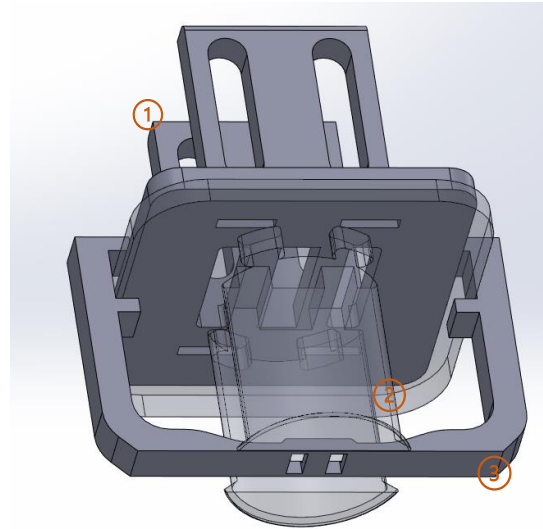


Figure 7: 1: Sensor positioning plate. 2: Coil support structure as shown in transparent mode. 3: Sensor fixing bracket.

4.2 Final Setup

In the final setup the GMR sensor was attached right below the coils, and both were mounted to the supporting beam. The GMR was attached to its independent regulated DC power supply and both the coil and GMR were connected to the lock-in amplifier. The grounding tape was grounded, and the test sample was placed on the sample pedestal. These can be seen in Figure 8. The lock-in amplifier was connected through serial port to a computer to store the collected data. Due to a data buffer in the lock-in amplifier of 8,192 bytes, the speed and sampling frequency were fixed based on the amount of data that could be collected by the lock-in amplifier.

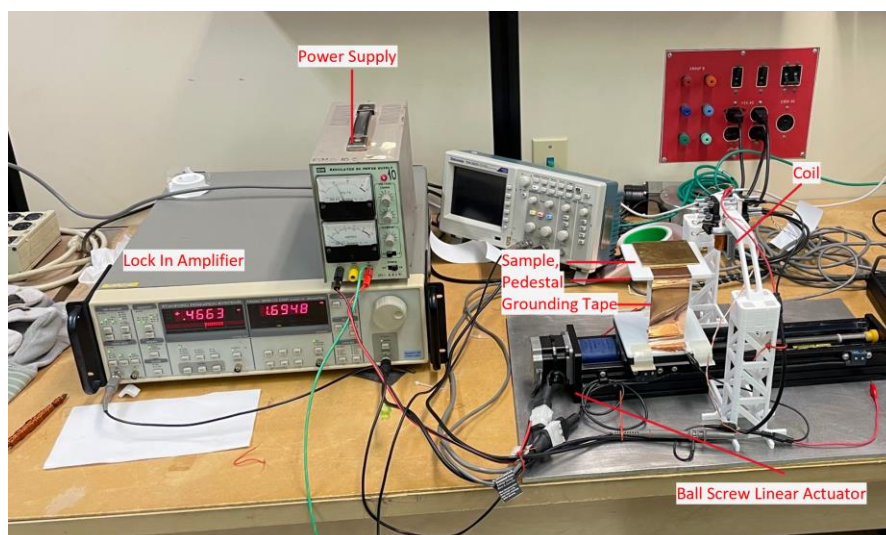


Figure 8: Finalized design for testing.

Once everything is setup a faraday cage was placed over the sensor as shown in Figure 9. A python script was used to control the Velmex BiSlide linear actuator to move the sample under the coils and sensor. This script also began taking recordings of the data that the lock-in amplifier was reading from the GMR sensor. After the linear actuator had moved the sample across the track, data collection stopped, and the results were graphed.



Figure 9: Finalized testing design with faraday cage

5.0 Results

Data was collected by scanning the plates of each metal in four configurations: big hole plate, small hole plate, plate with crack on underside, and a plate with a hole under a plate without defects. The figures show normalized voltage as a function of distance from start of first data point. The data from the aluminum shown in Figure 10.

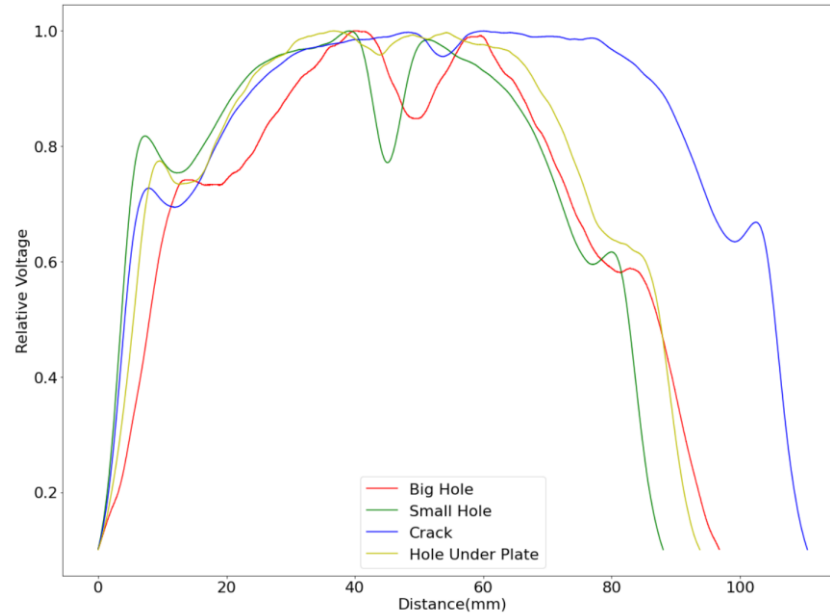


Figure 10: Normalized voltage reading as a function of distance for aluminum plates with a large hole, small hole, crack on underside of plate and a small hole under a defect free plate. A frequency of 2.765kHz was used to drive the coil for the big hole, small hole, and crack samples. A frequency of 1.6948kHz was use for the hole under plate sample.

An expanded view of the data collected from the aluminum plate with crack on the underside is show in Figure 11 below.

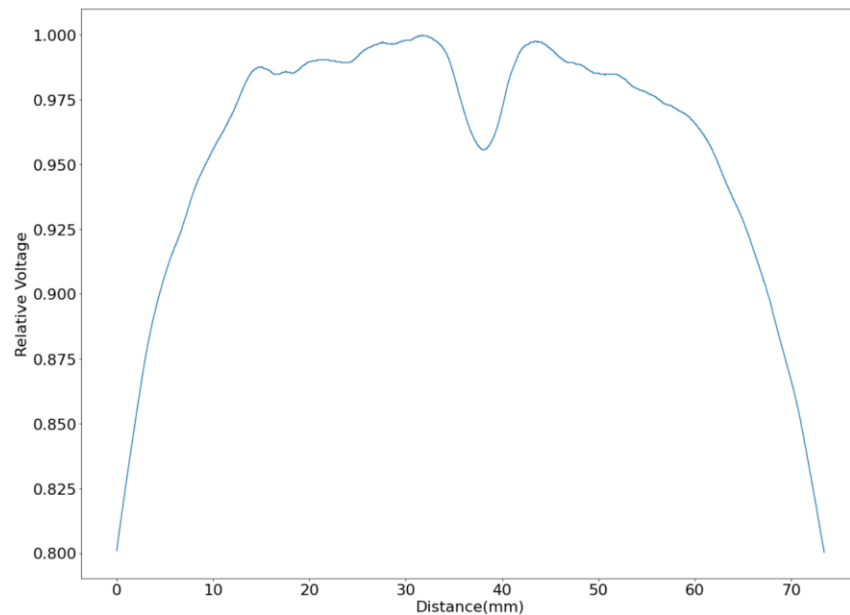


Figure 11: Focused view of normalized voltage data collected from the aluminum plate with crack on underside, the dip showing where the cut is located relative to the start of the data. A frequency of 2.765 kHz was use to drive the coil.

The data collected from the copper plates in the four configurations is shown in Figure 12

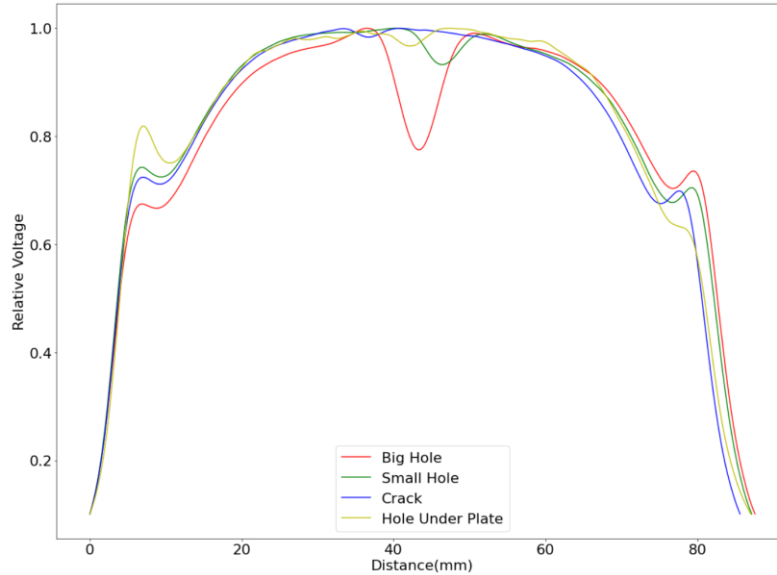


Figure 12: Normalized voltage reading as a function of distance for copper plates with a large hole, small hole, crack on underside of plate and a large hole under a defect free plate. A coil frequency of 2.841kHz was used for the big hole, small hole, and crack samples. A frequency of 1.6948kHz was use for the hole under plate sample.

An expanded view of the data collected from the plate with the crack on the underside is show in Figure 13.

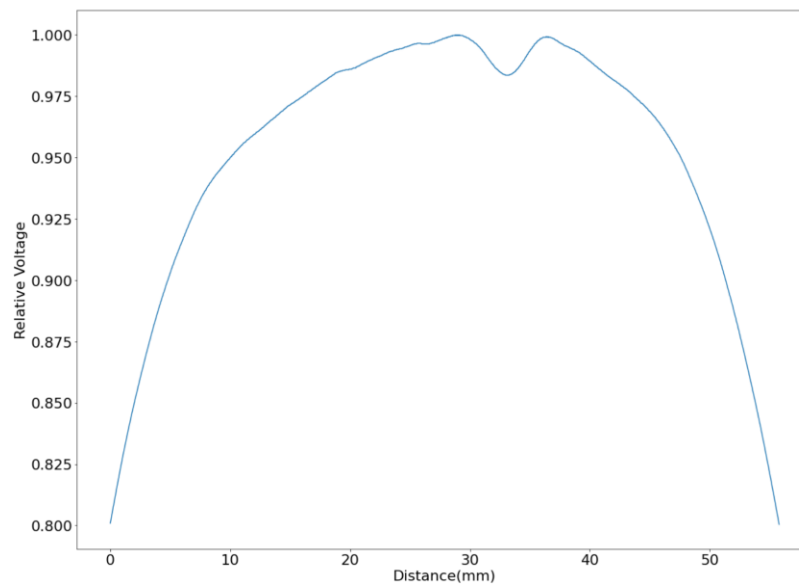


Figure 13: Focused view of normalized voltage data collected from the copper plate with crack on underside, the dip showing where the cut is located relative to the start of the data. A coil frequency of 2.841kHz was used.

Data from brass samples in similar configurations was collected and can be seen in Figure 14.

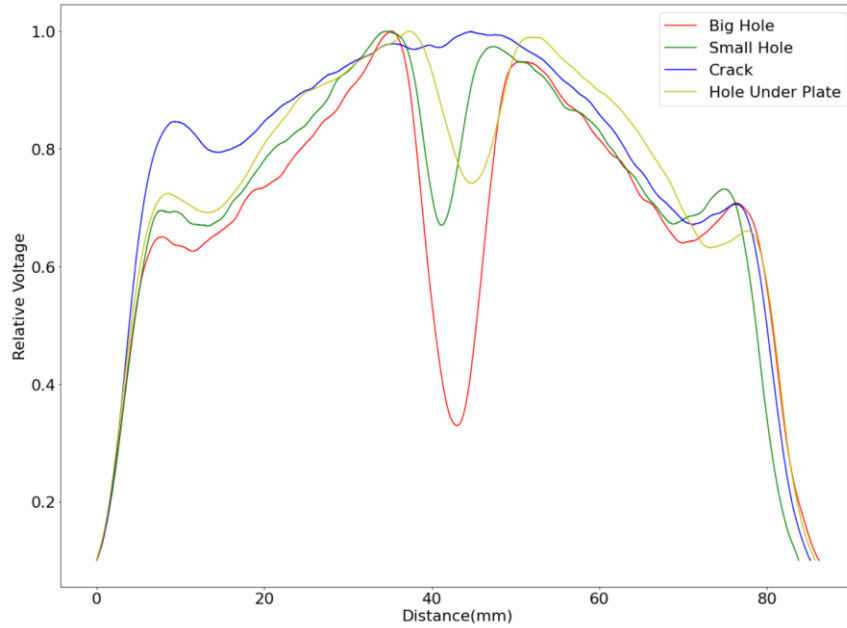


Figure 14: Normalized voltage reading as a function of distance for brass plates with a large hole, small hole, crack on underside of plate and a large hole under a defect free plate. A coil frequency of 1.6569kHz was used for the big hole, small hole and crack samples. A frequency of 1.6948kHz was use for the hole under plate sample.

An expanded view of the data for the brass plate with the two cracks on it is shown in Figure 15.

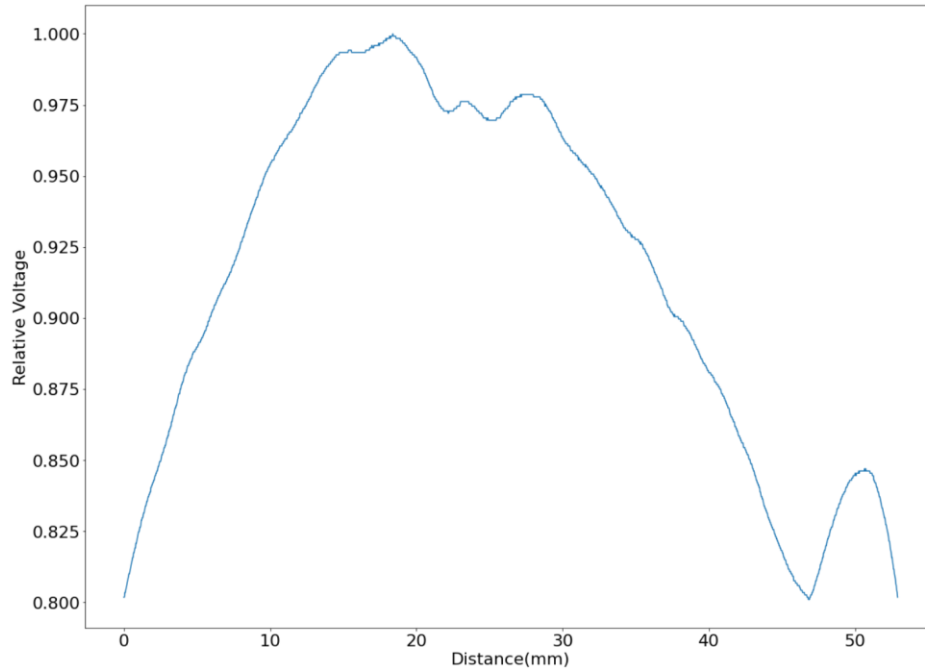


Figure 15: Focused view of normalized voltage data collected from the brass plate with crack on underside, the dips showing where the crack is located relative to the start of the data, and the double slit nature of the crack. A coil frequency of 1.6569 kHz was used.

Data collected for the aluminum large hole plate with the coil in the two different phase configurations and can be seen Figure .

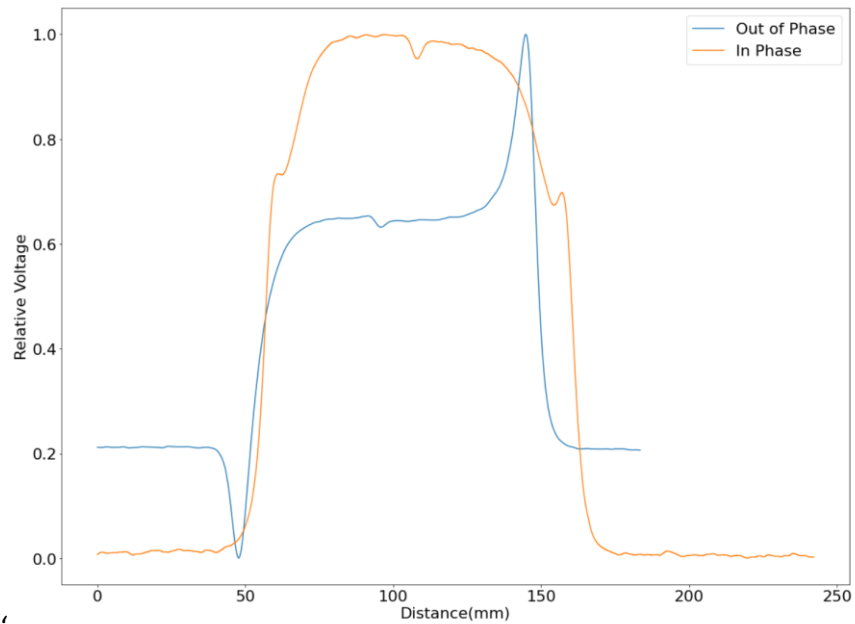


Figure 16: Shows normalized voltage vs distance offset data collected for the large hole aluminum plate with the coil in both the in-phase configuration and out of phase configuration. A coil frequency 2.765kHz was used.

Data for a basic 2D scan can be seen in Figure 17. Data was taken at three different points and then mirrored to show the general shape of the hole.

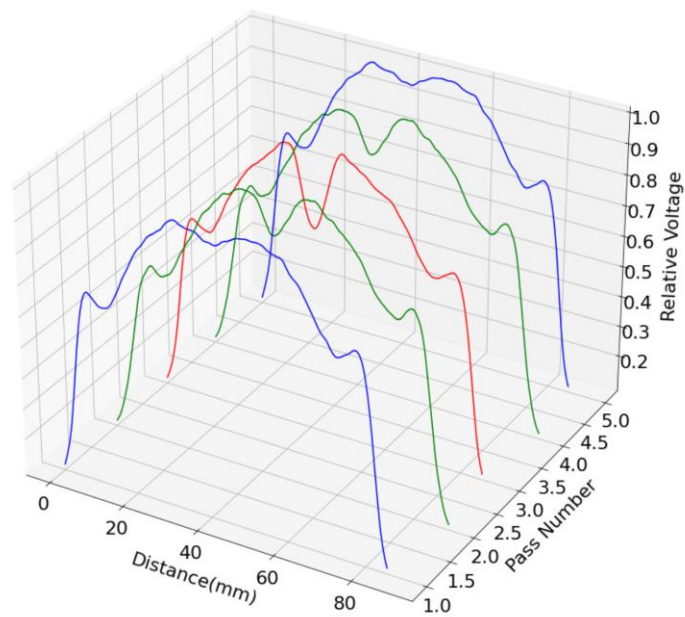


Figure 17: Show 3 scans at different distances away from the hole with pass numbers 4 and 5 being the same as 2 and 1 respectively. A coil frequency of 1.6948 kHz was used.

A scan was performed on the steel sample with a large hole, the data can be seen in Figure 18

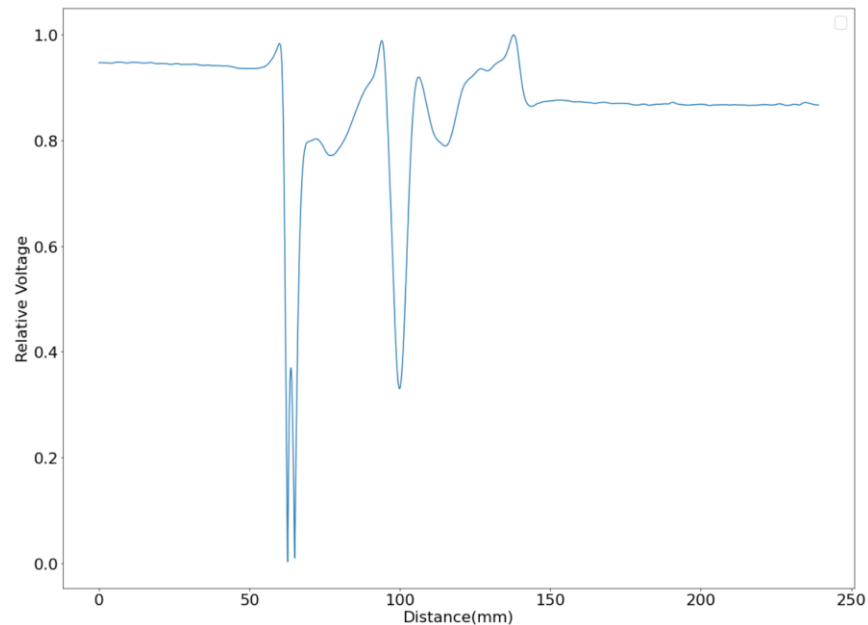


Figure 18: Normalized voltage vs distance offset from start of data for a steel plate with large hole. A coil frequency of 1.6569kHz was used.

6.0 Discussion

The results shown in Section 5.0 demonstrate that the sensor was able to detect surface and subsurface flaws in the copper, brass, and aluminum samples. These subsurface flaws included cracks that were on the underside of a plate, and holes that were underneath another plate. The smallest subsurface flaw that was detected was a 0.18mm crack in the aluminum sample seen in Figure 11. The sensor was able to detect the two cracks made in a brass plate and distinguish between them as seen in Figure 15. Although defects in metal deposition can be much smaller than this the project was overall successful in its goal of measuring subsurface flaws.

Currently the data is being analyzed by normalizing and comparing the difference in the measured magnetic field without considering the overall magnitude of the signal. This was done because the voltage magnitude was extremely sensitive to changes in setup and the various physical characteristics of the sample. This can be seen in Figure 10 where the big hole data appears to have a smaller magnitude than the small hole data. The big hole aluminum data was taken much earlier than the rest of the samples before various small changes were made to the setup such as the faraday cage and changes to frequency. The data was not retaken because the

large hole aluminum sample was damaged by being bent. This resulted in the distance between the sample surface and the sensor was not consistent throughout the test. This resulted in further scans having wild voltage reading making it nearly impossible to see the hole. Other large difference in voltage magnitude could be observed between runs with other metals, but after normalization the difference would minimize.

Both operational modes of the coil were considered during testing, generating two different geometries of magnetic fields. Although the out of phase method - where the magnetic field lines would run in parallel to the surface of the samples - displayed similar results in detecting the sample flaws, unanticipated end behavior occurred in the data corresponding to situations where the edge of the sample was aligned between the coils with a single coil residing over the sample, and the other completely off the sample surface (Seen in Figure 16). Due to this strange end behavior and similar results at the defect sites, it was decided to measure the sample using the in-phase method to capture better detection in flaws near the edges of the samples.

The steel sample with the large diameter hole shown in Figure 18 is drastically different than the other collected data. Although there is clear indication of the location of the defect in the sample, there is an unexplained voltage drop at the beginning of the sample, which is believed to occur due to magnetic effects. Although, no clear magnetic effects appeared in the sample in the presence of a bar magnet, it is believed the unexplained voltage drop may have occurred from magnetic dipole moments that occurred in the material at the start of

To continue this project towards the goal of real time eddy current testing in 3D printers, several next steps need to be taken. One of these would be to begin two-dimensional scanning of the samples. This would allow observation of the sample data to give coordinates of the defect's positions on a 2D plane. To do this accurately, a system would need to be created to move the sample in two dimensions as the current setup only allows 1D motion. A preliminary test of this was done by taking three scans of a piece of brass at different points to give a basic 2D model of the system. The offset scans were mirrored on either side to give a fuller graph that is a better approximation of the possible 2D system. This graph can be seen in Figure 17. A 2D data set would allow for better topographical analysis of the data which would allow the user to distinguish between subsurface cracks and holes in the samples, that would ultimately be required for actual metal deposition samples. By empirically fitting a relation between the

voltage drop, and the defect size for known defects such as the ones presented in this study, the size of unknown defects and cracks could be determined through this testing method. This would also lead to better indications of defect density, which was the inspiration of the project.

In order to be useful in the 3D printing process the sensor must be made more sensitive to smaller defects. The current setup is able to detect changes in the magnetic field equivalent to a fraction of a nanovolt, however the noise at this level makes it difficult to analyze. Further reduction of noise may be possible by reducing vibrations in the motor, steadying the stand and replacing the current wires with coaxial cables. In order to help in the detection of smaller defects, the area of detection must be made smaller. This can be done by making the coil smaller, but this would have negative drawbacks in fields strength, instead a magnetic core could be added. The magnetic core would act as a guide, strengthening and concentrated the field into an area that can be smaller than the diameter of the coil itself [2]. This would limit the magnetic field to act over a smaller portion of the surface, allowing for a more precise determination of where the flaws are.

In order to be used in the manufacturing of 3D printing, an apparatus would have to be designed to allow the sensor to scan layers inside the printer. The apparatus would have to be designed in such a way to allow for scanning during the printing process without significantly slowing it down. Along with the other improvements, real time flaw detection in 3D printing could be realized.

8.0 Economic Analysis

A brief overview of the cost breakdown for the project is given in the tables below.

8.1 Sensor Materials

Table 1: Cost of materials used for the sensor. The Linear Actuator and Lock-in Amplifier were provided by the Queen's University Physics Lab.

Materials	Cost
Linear Actuator (Velmax BiSlide)	\$562 [10]
Lock-In Amplifier (SR810)	\$4250 [11]
GMR Sensor (AAL002-02E)	\$30.23 [7]
Copper Wire	Negligible
TOTAL	\$4842.23

8.2 Testing Materials

Table 2: Cost of materials used in the testing process

Materials	Cost
3d printed parts	\$16.33 Table 5 and 6 in appendix
Faraday cage	\$30
Test Samples	\$63.00
TOTAL	\$109.33

9.0 Conclusion

In the goal of detecting surface and subsurface flaws in thin layers of 3D printed metals, an ECT apparatus was designed and constructed. Design decisions were made to enable optimal measurements for these detections. For instance, a GMR sensor was chosen to increase the maximum tolerable frequency that could be used to drive the eddy currents, thus decreasing the penetration depths. Mirrored coils were used as opposed to a single coil to allow the induction of eddy currents from magnetic fields of two separate orientations as opposed to one. Testing was conducted by sliding samples underneath a GMR and coil. The results showed detection of both subsurface cracks and holes both on and below the surface. As expected, detection was more pronounced for larger holes. It was also more pronounced for small holes on the surface than for large holes about a millimeter below the surface. Detection of subsurface cracks was the weakest. The detection of these surface and subsurface flaws is significant by itself, but more work needs to be done to allow for its use in 3D metal printing. There are several next steps that could be pursued to improve upon and extend the work done in this project and prepare eddy current testing to be incorporated in 3D printers. These include more substantial 2D surface scanning, increased detection sensitivity, and the building of an attachment apparatus. Once realized, accurate real-time detection of flaws in metals as they are being manufactured could result in significant savings of time and money during the manufacturing process, and should be pursued further.

References

- [1] "Typical Defects of 3D Printed Metal Parts - Eplus3D." https://www.eplus3d.com/Company-News/article_177 (accessed Sep. 27, 2021).
- [2] D. J. Griffiths, *Introduction to Electrodynamics*, 4th ed. Prentice Hall, 1999. Accessed: Dec. 05, 2021. [Online]. Available: <http://himafi.fmipa.unej.ac.id/wp-content/uploads/sites/16/2018/09/Introduction-to-Electrodinamic.pdf>
- [3] "Eddy Current Testing Probe Based on Double-Coil Excitation and GMR Sensor | IEEE Journals & Magazine | IEEE Xplore." <https://ieeexplore.ieee.org/document/8624304> (accessed Dec. 05, 2021).
- [4] NVE Corporation, "How GMR Works," *How GMR Works*. <https://www2.nve.com/gmrsensors/gmr-operation.htm> (accessed Nov. 02, 2021).
- [5] Physics and Radio Electronics, "TMR," *Magneto Resistor*. <https://www.physics-and-radio-electronics.com/electronic-devices-and-circuits/passive-components/resistors/magnetoresistor.html>
- [6] H. Malekmohammadi, A. Migali, S. Laureti and M. Ricci, "A Pulsed Eddy Current Testing Sensor Made of Low-Cost Off-the-Shelf Components: Overview and Application to Pseudo-Noise Excitation," in *IEEE Sensors Journal*, vol. 21, no. 20, pp. 23578-23587, 15 Oct.15, 2021, doi: 10.1109/JSEN.2021.3108519.
- [7] "AAL002-02E NVE Corp/Sensor Products | Sensors, Transducers | DigiKey." <https://www.digikey.ca/en/products/detail/nve-corp-sensor-products/AAL002-02E/1624603> (accessed Dec. 05, 2021).
- [8] "LF21215TMR Littelfuse Inc. | Sensors, Transducers | DigiKey." <https://www.digikey.ca/en/products/detail/littelfuse-inc/LF21215TMR/11200040?s=N4lgjCBcoLQBxVAYygMwIYBsDOBTANCAPZQDa4CAugL7WEBMZIAMgGL1gcCsAKgLIAIEDSA> (accessed Dec. 05, 2021).
- [9] "What's the Layer Thickness of the Different 3D Printing Materials? | Help Center | i.materialise." <https://imaterialise.helpjuice.com/materials/layer-thickness> (accessed Dec. 05, 2021).
- [10] "Motorized BiSlide Systems - Velmex." https://www.velmex.com/Products/BiSlide/BiSlide_Motorized.html (accessed Dec. 05, 2021).
- [11] "SRS Online Ordering." <https://orders.thinksrs.com/OnlineOrders/SRSOrders.html?EPrdGrp=SR810> (accessed Dec. 05, 2021).

Appendices

Appendix A: Models

The following code was used to model the system for obtaining a desired coil shape.

```
L = L/2
n = N/L
Bx = mu0*n*I/2*((x+L)/(np.sqrt((x+L)**2 + R**2))) - ((x-L)/(np.sqrt((x-L)**2 + R**2)))
return (Bx)

def plotB():
    plt.plot(x, Bfield(mu, N, 1, R, 3e-2, x))
    plt.title('B field as function of distance from sample', fontsize = 16)
    plt.xlabel('Distance from sample', fontsize = 16)
    plt.ylabel('B-field', fontsize = 16)
    # plt.ylim(-1e-4, 1e-4)
    plt.show()
```

plotB()



Figure 1

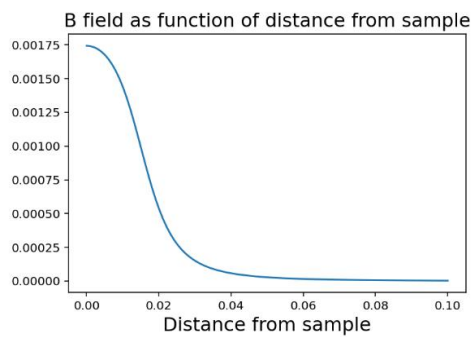


Figure 19: Python script used to model the field strength of metal coil as a function of distance from the sample surface.

```

def Bfield(mu0, N, I, R, L, x):
    L = L/2
    n = N/L
    Bx = mu0*n*I/2*((x+L)/(np.sqrt((x+L)**2 + R**2))) - ((x-L)/(np.sqrt((x-L)**2 + R**2)))
    return (Bx)

def plotBR():
    plt.plot(R, Bfield(mu, N, 1, R, 3e-2, 2.5e-3))
    plt.title('B field as function of coil radius', fontsize = 16)
    plt.xlabel('coil radius', fontsize = 16)
    plt.ylabel('B-field', fontsize = 16)
    # plt.ylim(-1e-4, 1e-4)
    plt.show()

```

plotBR()

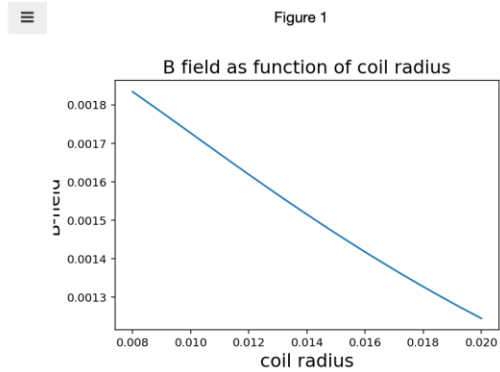


Figure 20: Python script used to model the field strength of metal coil as a function of coil radius.

Appendix B: Printer Settings and Materials Cost

Table 3: Slicer used for the 3D printing, printer model, nozzle stats, filament type, print quality and slicer setting for the supporting structure.

Slicer	Ultimaker Cura 4.11.0
3D Printer	Creality Ender 5 Plus
Nozzle	0.4mm brass nozzle came with the printer
Filament	Creality white PLA
Print Quality	Standard Quality 0.2 mm layer thickness
Wall thickness	Wall thickness 2mm
Top and bottom thickness	top and bottom 1mm
Infill percentage	20% line pattern
Infill overlap	30%

Link to the filament:

https://www.amazon.ca/gp/product/B07PMN9Z2Q/ref=ppx_yo_dt_b_asin_title_o00_s00?ie=UTF8&psc=1

\$31.99 for 1kg

Table 4: Slicer used for the 3D printing, printer model, nozzle stats, filament type, print quality and slicer setting for the sensor fixing components.

Slicer	PrusaSlicer 2.3.3
3D Printer	Prusa i3 MK3S+
Nozzle	0.4mm nozzle came with the printer
Filament	Prusa PLA galaxy grey
Print Quality	0.2 mm layer thickness
Wall thickness	Wall thickness 2mm
Top and bottom thickness	top and bottom 1mm
Infill percentage	20% line pattern for coil structure, 100% infill for sensor bracket
Infill overlap	30%

Table 5: Parts printed with Creality white PLA weight and cost

Parts	Weight total (g)	Cost (\$)
Pillars*2	236.8	7.58
Beam	70.5	2.11
Hanging plate	15.8	0.51
Sample plate	43.4	1.39
Sample support	77.9	2.49
Height adjust thread	44.7	1.43
Threads*2	1.4	0.04

Nuts*2	3.4	0.11
Stoppers	1.1	0.04
Total	495	15.7

Table 6: Parts printed with Prusa Galaxy Grey weight and cost

Parts	Weight total (g)	Cost (\$)
Coil structure	15.83	0.477
Sensor bracket	4.90	0.15
Total	20.73	0.627

[Creality Official PLA 3D Printer Filament, Dimensional Accuracy +/- 0.03 mm, 2.2 LBS \(1.0KG\), 1.75 mm, White : Amazon.ca: Everything Else \\$31.99](#)

Appendix C: Data Acquisition Code:

```
import serial

class lockin: #class for communicating with the motor controller
    def __init__(self,port):
        self.lok = serial.Serial(port, baudrate=19200, parity=serial.PARITY_NONE,
stopbits=serial.STOPBITS_ONE, bytesize=serial.EIGHTBITS, timeout=3)

    def ask(self,cmd):
        self.lok.write(cmd+b'\n')
        self.lok.flush()
        idn = self.lok.readline()
        print("%s" %(idn))
        return idn

    def send(self,cmd):
        self.lok.write(cmd+b'\n')
        self.lok.flush()

    def __exit__(self):
        self.lok.close()

class motor: #class for communicating with the lock in amplifier
    def __init__(self,port):
        self.mot = serial.Serial(port, baudrate=9600, parity=serial.PARITY_NONE,
stopbits=serial.STOPBITS_ONE, bytesize=serial.EIGHTBITS, timeout=3)

    def ask(self,cmd):
        self.mot.write(cmd+b'\n')
        self.mot.flush()
        idn = self.mot.readline()
        print("%s" %(idn))
        return idn

    def send(self,cmd):
        self.mot.write(cmd+b'\n')
        self.mot.flush()

    def read(self):
        idn = self.mot.readline()
        print("%s" %(idn))
        return idn

    def __exit__(self):
        self.mot.close()
```

```
ln = lockin("COM1") #set the lock in port to COM1
mT = motor("COM5") #sets the motor port to COM5
ln.send(b'REST') #clears the buffer in the locking
ln.send(b'SRAT10') #set the data collection rate
ln.send(b'OFLT9') #sets the time constant for the averaging
mT.ask(b'E') #set the motor control to be controlled by computer and echo
commands
mT.ask(b'C') #clears the previous program
mT.ask(b'S1M400,I1M-60000,R') #tells the motor to move from one end to the other
at a certain speed
#this section determines if the motor is still moving
motStatus = b'B'
ln.send(b'STRT') #starts collecting data
while (motStatus == b'B'):
    motStatus = mT.ask(b'V')
ln.send(b'PAUS') #pauses the collection of data
mT.send(b'Q')
del mT
ln.send(b'PAUS') #pauses the collection of data
N = ln.ask(b'SPTS?') #asks for the number of data points in data buffer
data = ln.ask(b'TRCA?0,'+N) #asks to send the data points back to the
del ln #free port 5
```